

On the interdependence of galaxy morphology, star formation, and environment in massive galaxies in the nearby Universe

Omkar Bait,¹[★] Sudhanshu Barway,²[†] and Yogesh Wadadekar¹[‡]

¹*National Centre for Radio Astrophysics, Tata Institute of Fundamental Research, Post Bag 3, Ganeshkhind, Pune 411007, India*

²*South African Astronomical Observatory, P.O. Box 9, 7935, Observatory, Cape Town, South Africa*

Accepted XXX. Received YYY; in original form ZZZ

ABSTRACT

Using multi-wavelength data, from UV-optical-near-mid IR, for ~6000 galaxies in the local Universe, we study the dependence of star formation on the morphological T-types for massive galaxies ($\log M_*/M_\odot \geq 10$). We find that, early-type spirals (Sa-Sbc) and S0s predominate in the green valley, which is a transition zone between the star forming and quenched regions. Within the early-type spirals, as we move from Sa to Sbc spirals the fraction of green valley and quenched galaxies decreases, indicating the important role of the bulge in the quenching of galaxies. The fraction of early-type spirals decreases as we enter the green valley from the blue cloud, which coincides with the increase in the fraction of S0s. This points towards the morphological transformation of early-type spiral galaxies into S0s which can happen due to environmental effects such as ram-pressure stripping, galaxy harassment, or tidal interactions. We also find a second population of S0s which are actively star-forming and are present in all environments. Since morphological T-type, specific star formation rate (sSFR), and environmental density are all correlated with each other, we compute the partial correlation coefficient for each pair of parameters while keeping the third parameter as a control variable. We find that morphology most strongly correlates with sSFR, independent of the environment, while the other two correlations (morphology-density and sSFR-environment) are weaker. Thus, we conclude that, for massive galaxies in the local Universe, the physical processes that shape their morphology are also the ones that determine their star-forming state.

Key words: galaxies: evolution — galaxies: star formation — galaxies: statistics — galaxies: structure — galaxies: general — galaxies: groups: general

1 INTRODUCTION

Galaxies are broadly classified, based on their visual morphologies, into ellipticals (Es), lenticulars (S0s), spirals and irregulars (Hubble 1926). Remarkably, various physical parameters (in terms of size, optical colors, luminosity, HI mass fraction, etc.) of galaxies are known to correlate with morphology (Roberts & Haynes 1994). The average star formation rate (SFR) also shows a strong trend with morphology, with a low rate of star formation in Es and S0s, and increasing as we go to spiral galaxies (Kennicutt 1998).

With the advent of large area galaxy surveys, like the Sloan Digital Sky Survey (SDSS, York et al. (2000)), it was

found that in the local Universe, galaxies show a bi-modal distribution on the optical color-magnitude diagram (Stratava et al. 2001; Kauffmann et al. 2003a; Baldry et al. 2004, 2006) with actively star forming “blue cloud” galaxies and passively evolving “red sequence” galaxies. The region between these two populations is defined as the “green valley” (Wyder et al. 2007). It is believed that the green valley of galaxies is the transition zone between the blue cloud and the red sequence (Wyder et al. 2007; Schiminovich et al. 2007; Mendez et al. 2011), and contains galaxies that have undergone recent quenching of star formation (Salim et al. 2007). Along with the star-formation properties, green valley galaxies also have morphological properties (quantified by the value of the Sérsic index) intermediate between star-forming and passive galaxies (Schiminovich et al. 2007). Thus, green valley galaxies can give us insight into the process of quench-

[★] E-mail: omkar@ncra.tifr.res.in (OB)

[†] E-mail: barway@sao.ac.za (SB)

[‡] E-mail: yogesh@ncra.tifr.res.in (YW)

ing and its dependence on morphology and other galaxy parameters.

Further, galaxies also show a correlation between their star formation rate (SFR) and stellar mass, the so-called ‘main-sequence’ of star-forming galaxies (MS), both in the local Universe (Brinchmann et al. 2004; Salim et al. 2007) and at high redshifts of up to 2 (Daddi et al. 2007; Elbaz et al. 2007; Noeske et al. 2007; Peng et al. 2010). Star-forming galaxies can lose their position on the MS due to various physical processes giving rise to a population of passively evolving galaxies. The exact cause for the cessation of star formation under different physical conditions is still heavily debated. Phenomenological studies of quenching have indicated that there are two completely separable processes: ‘mass quenching’ by which star-forming galaxies undergo rapid quenching above the Schechter mass (M^*), and ‘environmental quenching’ which produces a second component of quenched galaxies at the lower mass end (Baldrý et al. 2006; Peng et al. 2010). Various physical mechanisms are invoked to explain quenching e.g., halo-quenching (Dekel & Birnboim 2006), morphological quenching (Martig et al. 2009), AGN-feedback (Croton et al. 2006), strangulation (Larson et al. 1980), ram-pressure stripping (Gunn & Gott 1972), and harassment (Farouki & Shapiro 1981; Moore et al. 1996).

Several studies have also shown that the passive state of a galaxy correlates strongly with the internal structure of a galaxy e.g., with stellar surface mass density (Kauffmann et al. 2003b), in particular with $\Sigma_{1 \text{ kpc}}$, the inner 1 kpc stellar surface mass density (Cheung et al. 2012; Fang et al. 2013; Woo et al. 2015) or with bulge mass (Bluck et al. 2014) and also with σ , the central velocity dispersion (Wake et al. 2012; Teimoorinia et al. 2016). Such a correlation is more strong for the central galaxy in a dark matter halo than for satellites. Omand et al. (2014) have shown that quenching depends both on the stellar mass and the effective radius R_e . It is important to note that these correlations may not necessarily mean that there is a causal connection between the quenching process and galaxy structural parameters. Lilly & Carollo (2016) have shown using a simple toy model that such correlations can naturally arise if we consider the Peng et al. (2010) mass-quenching model along with the observed redshift evolution of mass-size relation for star-forming galaxies. Moreover, the passive fraction also shows dependence on halo mass (Weinmann et al. 2006; Wetzel et al. 2012; Woo et al. 2013, 2015). Further, Schawinski et al. (2014) found that in the green valley, early type galaxies undergo rapid quenching whereas the late-type galaxies undergo a slow quenching process.

Since finding the visual morphologies of millions of galaxies from large scale galaxy surveys is difficult, several recent studies on star formation have mostly ignored the morphologies of galaxies. Galaxy Zoo (Lintott et al. 2008) has classified the morphologies of a large number of galaxies, but gives a crude classification in terms of only late-type (which includes all types of spiral galaxies) and early-type (ellipticals and S0s) galaxies. On the contrary, in our study we use the detailed visual morphologies (in 12 types – ellipticals, S0-, S0, S0/a, Sa, Sab, Sb, Sbc, Sc, Scd, Sd) from the Nair & Abraham (2010) catalogue, and hence we can distinguish between different kinds of spiral galaxies. We can also

differentiate between ellipticals and S0s which the Galaxy Zoo morphologies do not.

In this paper, we want to revisit the relation between classical visual morphologies and star formation in the modern context of the MS of star-forming galaxies, the transitioning population of green valley galaxies, and the quenched galaxies, and also as a function of environment from the low to high densities. We use multiwavelength data from UV-optical-mid IR and model the SED of ~ 7000 galaxies to estimate the stellar mass and SFRs. Due to the availability of UV data we can also define a green valley. In particular, we want to study the relation between sSFR-morphology, morphology-density, and density-sSFR. Since all three of the parameters, morphological T-type, sSFR, and environmental density are known to correlate with each other, in each of the correlations we also study the differential effect of the third parameter. Further, in order to determine which correlation is the strongest, we compute the partial correlation coefficient for each of the three correlations while keeping the third parameter as the control variable.

Our paper is organised as follows. In Section 2, we discuss our sample selection and our multiwavelength data from UV-optical-IR. We then briefly discuss the spectral energy distribution (SED) fitting technique using which we derive the stellar mass and SFR for our whole sample. We also discuss the morphological classifications and environmental density measurements for our whole sample. We then show our results and discuss them in Section 3. Our main results on the relation between star formation and morphology are in Section 3.1. In Section 3.2, we study the morphology-density relation for our sample of galaxies and separately study this relation for star-forming, green valley and quenched galaxies. In Section 3.3, we study the relation between the remaining two parameters, log sSFR and environmental density. In Section 3.4, we then analyse which correlation between the three parameters, morphological T-type, sSFR, and environmental density is strongest by computing the partial correlation coefficient. Finally, we summarize our results and conclude in Section 4.

Throughout this paper we use the standard concordance cosmology with $\Omega_M = 0.3$, $\Omega_\Lambda = 0.7$ and $h_{100} = 0.7$.

2 SAMPLE SELECTION AND DATA ANALYSIS

2.1 Sample selection

Our sample is drawn from the Nair & Abraham (2010) (hereafter NA10) catalogue of detailed visual morphological classification of 14,034 galaxies. NA10 galaxies were selected from the Sloan digital sky survey (SDSS) DR4 with spectroscopic redshift in the range $0.01 < z < 0.1$, and extinction corrected apparent magnitude limit of $g < 16$ mag. For galaxies in our sample, we use optical imaging data from the SDSS DR12 (Alam et al. 2015) in u, g, r, i , and z bands. In order to have a better constraint on recent star formation, we make use of Galaxy Evolution Explorer (GALEX) data in the far-UV (FUV) and near-UV (NUV) filters. We use near-IR data from the 2 Micron All Sky Survey (2MASS) in J, H , and K bands (Skrutskie et al. 2006), wherein we use the model photometry. Mid IR data are taken from the

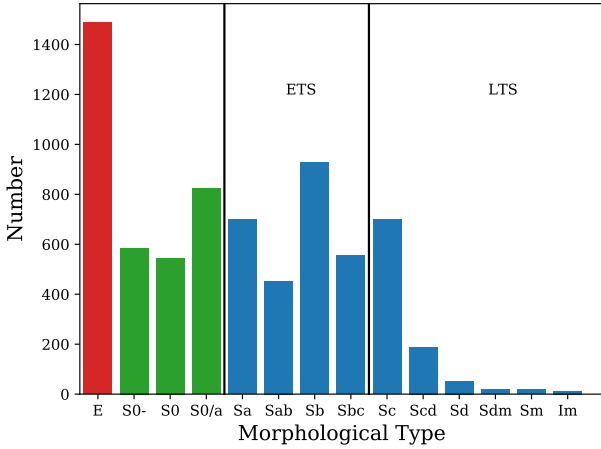


Figure 1. Number of galaxies in our sample with various morphologies, ranging from Es (red), S0s (green), and spirals (blue). We group together spirals ranging from Sa-Sbc and refer to them as early-type spirals (ETS), and Sc-Sd types which we refer as late-type spirals (LTS). Since we have only massive galaxies in our sample, we have very few number of late-type spiral galaxies. Sdm, Sm, and Im morphologies are removed from our final sample.

Wide-Field Infrared Survey Explorer (WISE; Wright et al. (2010)) in all four channels - W1, W2, W3, and W4. We construct our sample by cross-matching the NA10 catalogue with archival data from GALEX, SDSS, 2MASS, and WISE which gives us 7,831 galaxies. Of these, we have flux measurements in all the 14 bands for 6,819 galaxies. For 594 galaxies we have flux measurements in 13 bands due to missing flux in the W4 filter, and for 418 galaxies we have flux measurement in 10 bands due to missing fluxes in all the 4 WISE filters. For all of these galaxies, we also have local environmental density information from Baldry et al. (2006).

All our sources are resolved in the four WISE bands and are also associated with the 2MASS extended source catalogue, hence we calculate the fluxes using elliptical aperture photometry measurement (w?gmag column in the WISE catalogue). Furthermore, the WISE pipeline measurements for resolved sources are known to be systematically fainter by approximately 0.35 mag, 0.28 mag, 0.44 mag and 0.3 mag in the W1, W2, W3 and W4 band respectively, and we correct for these offsets¹ (Brown et al. 2014) before calculating the fluxes. After these corrections are made, as mentioned in the WISE documentation¹, these fluxes still have an error of ~20%.

2.2 Morphological Classification

The visual morphologies in our final sample are taken from our parent sample of NA10. In NA10 the authors have done a careful morphological classification for every galaxy using SDSS images in all the five bands u, g, r, i, and z. NA10 can

differentiate between different kinds of spirals galaxies into Sa, Sab, Sb, Sbc, Sc, Scd, Sdm, Sm, and Im. It can also differentiate between lenticular galaxies into S0-, S0, and S0/a. Galaxies from NA10 which have somewhat doubtful classification (denoted by ?), and galaxies with highly uncertain classification (denoted by :) are not included in our sample. The comparison of the morphological classification from NA10 with the RC3 catalogue (de Vaucouleurs et al. 1991) is shown in Table 1. Since NA10 does not differentiate between c0, E0, and E+ we group them together into ellipticals (Es). Similarly, NA10 does not differentiate between S0 and S0+ morphologies and hence we group them together and refer them as S0. Thus, in our classification scheme, we have three types of lenticular galaxies, S0-, S0, and S0/a. Figure 1, shows the number of galaxies for each of the morphological classes in our sample. We have very few galaxies from Sdm-Im morphologies since our sample contains only massive galaxies and hence we remove them from our sample. This reduces our sample to 7,763 galaxies. The authors in NA10 have classified their entire sample twice and have estimated a mean deviation of less than 0.5 T-types.

We will use such a detailed morphological classification only in Section 3.1.3. For all other sections we will group together all types of lenticular galaxies (S0-, S0, and S0/a) and refer them as S0s. And within spiral galaxies we make two groups: early-type spirals (ETS) ranging from Sa-Sbc types, and late-type spirals (LTS) ranging from Sc-Sd types.

2.3 Deriving stellar masses and SFRs using SED fitting

For each of the 7,763 galaxies in our sample, we model the SED, using the publicly available Multi-wavelength Analysis of Galaxy Physical Properties (MAGPHYS) code (da Cunha et al. 2008) (dC08 hereafter). We will briefly describe the SED modeling done by MAGPHYS here; for a detailed description, we refer the reader to dC08.

MAGPHYS creates a library of template spectra and finds the best-fit spectrum to the available data in UV, optical, near and mid IR bands. MAGPHYS uses “CB07 library”, which is the unpublished version of the Bruzual & Charlot (2003) stellar population synthesis model, with a Chabrier initial mass function. A set of optical library templates are constructed, by varying the star formation history, which is modeled as an exponentially decaying star formation rate with random bursts of star formation superimposed on it, and also by varying metallicity from 0.02 to 2 times solar metallicity. The two-component Charlot & Fall (2000) model is used to estimate the amount of dust attenuation. In this model, the dust attenuation is higher around young stars (age < 10⁷ Myr) as they are born in dense molecular clouds. MAGPHYS then performs a χ^2 fit on the given data, say in UV, optical, and IR bands with the entire library of template SEDs. For each parameter in the model, MAGPHYS also builds a likelihood distribution by weighting the parameter value with the probability given by $\exp(-\chi^2/2)$. We use the median values (the 50th percentile of the marginalized posterior probability distribution function) of stellar mass and SFR for each galaxy in our sample (cf. dC08). For every galaxy we also estimate the uncertainty in estimating the stellar mass and SFR using the 16th and 84th percentile of the marginalized posterior probability distribution, which

¹ http://wise2.ipac.caltech.edu/docs/release/allsky/expsup/sec6_3e.html

Table 1. Corresponding morphological T-types from the NA10 and RC3 catalogues.

Class	c0	E0	E+	S0-	S0	S0+	S0/a	Sa	Sab	Sb	Sbc	Sc	Scd	Sd	Sdm	Sm	Im
NA10	-5	-5	-5	-3	-2	-2	0	1	2	3	4	5	6	7	8	9	10
RC3	-6	-5	-4	-3	-2	-1	0	1	2	3	4	5	6	7	8	9	10

will be the lower and upper error bars respectively, following dc08. As we lack observations around the 100 micron dust peak, we are unable to constrain the emission from cold dust, and hence we refrain from using dust mass and dust luminosity in our analysis.

We used the MAGPHYS SED fitting technique to model the individual SED using 14 bands, ranging from UV-midIR, of 7,763 galaxies in our sample. Following [Smith et al. \(2012, Eq. B2\)](#), for a data set of 14 bands, the number of degrees of freedom is 8. This corresponds to a critical χ^2 of 20, above which there is less than 1 percent probability that our observations are consistent with the models. However, following the suggestion of [Hayward & Smith \(2015\)](#) of using a more conservative value than that derived from [Smith et al. \(2012\)](#), we use a critical χ^2 of 5, and remove all galaxies with higher χ^2 from our sample. This criterion reduces the sample to 7020 galaxies. Figure 2 is a typical example of a good fit SED in our sample. Notice that due to lack of data points the polycyclic aromatic hydrocarbon (PAH) emission features and FIR dust emission are not very well constrained.

Figure 3, shows the histogram of stellar mass for the sample for 7020 galaxies. As our focus in this paper is only on massive galaxies and their dependence on sSFR, morphology and environment. Hence, we restrict our sample to only massive galaxies ($\log M_*/M_\odot \geq 10$). The dashed vertical line in Figure 3 shows the stellar mass cut. This finally reduces our sample to 6194 galaxies, which we will use in this work. We caution the reader that the results presented in this paper are valid only for massive galaxies; these could significantly change for lower mass galaxies, where different physical processes may play a role in shaping their nature. Figure 4, shows the distribution of sSFR for our final sample. The sSFR is obtained by dividing the SFR by the stellar mass for each galaxy. The sSFR is a proxy for the star formation history of the galaxy, where a high value of sSFR suggests recent star formation and a low value is an indicator of an older stellar population with little or no recent star formation. Therefore, following [Salim \(2014\)](#), we define star-forming galaxies with $\log \text{sSFR} \geq -10.8$, green valley galaxies with $-11.8 < \log \text{sSFR} < -10.8$, and quenched galaxies with $\log \text{sSFR} \leq -11.8$.

2.4 Environmental Density

We use the local surface galaxy density from [Baldry et al. \(2006\)](#) as a measure of the environment. It is determined using, $\Sigma_N = N/\pi d_N^2$, where d_N is the distance to the Nth nearest neighbour which are within the redshift range $\pm \Delta z c = 1000 \text{ km/s}$ for galaxies with spectroscopic redshifts or within the 95% confidence limit for galaxies with photometric redshifts only. Following [Baldry et al. \(2006\)](#), we use the best estimate, Σ , obtained by averaging the Σ_N for the 4th and

5th nearest neighbour. Figure 5 shows the histogram of $\log \Sigma$ for our final sample of galaxies. Further we split our sample into low density ($\log \Sigma (\text{Mpc}^{-2}) < -0.5$), intermediate density ($-0.5 < \log \Sigma (\text{Mpc}^{-2}) < 0.5$), and high densities ($\log \Sigma (\text{Mpc}^{-2}) > 0.5$).

We provide the MAGPHYS output along with information on morphology, and environmental density from NA10, for our sample of galaxies in the form of a catalogue. Table 2 shows a sub-sample of the catalogue; the full table is available in the electronic version of this paper.

3 RESULTS AND DISCUSSION

Galaxy morphology, sSFR, and environmental density are correlated with each other. It is possible that the correlation between any two of the parameters is driven by the dependence on the third parameter. Hence, in each of the following subsections we study the correlation between any two of the parameters along with the differential effect of the third parameter. We also compute the partial correlation coefficient for each the three correlations while keeping the third parameter as the control variable.

3.1 Relation between morphology and specific star-formation rate

In this section, we study the dependence of morphology on the sSFR- M_* plane. We then examine the fraction of galaxies of different morphologies at fixed sSFR, and also the differential effect of environment on it.

3.1.1 Dependence of morphology on the sSFR- M_* plane

We plot sSFR and stellar mass (M_*) for our sample in the left panel of Figure 6. Most of the galaxies in our sample have a redshift below 0.07, and hence mass-incompleteness is not a major issue. We nevertheless correct for the mass-incompleteness in the sample using the $1/V_{max}$ method ([Schmidt 1968](#)). In this method we simply weight each galaxy by the maximum volume it can be detected referred by V_{max} . The weight for each galaxy is then $1/V_{max}$. We use the $1/V_{max}$ provided by the NA10 catalogue for every galaxy in our sample. In the left panel of Figure 6 the contours shows the $1/V_{max}$ -corrected density of galaxies on the stellar mass and sSFR plane. On the top-right corner the error bars shows the typical uncertainties in the estimation of stellar mass and sSFR. In order to estimate the typical uncertainty, we first find the median value of both the 16th and 84th percentile from the marginalized posterior probability distribution function for each parameter. And then take the mean of these two values which represent the error

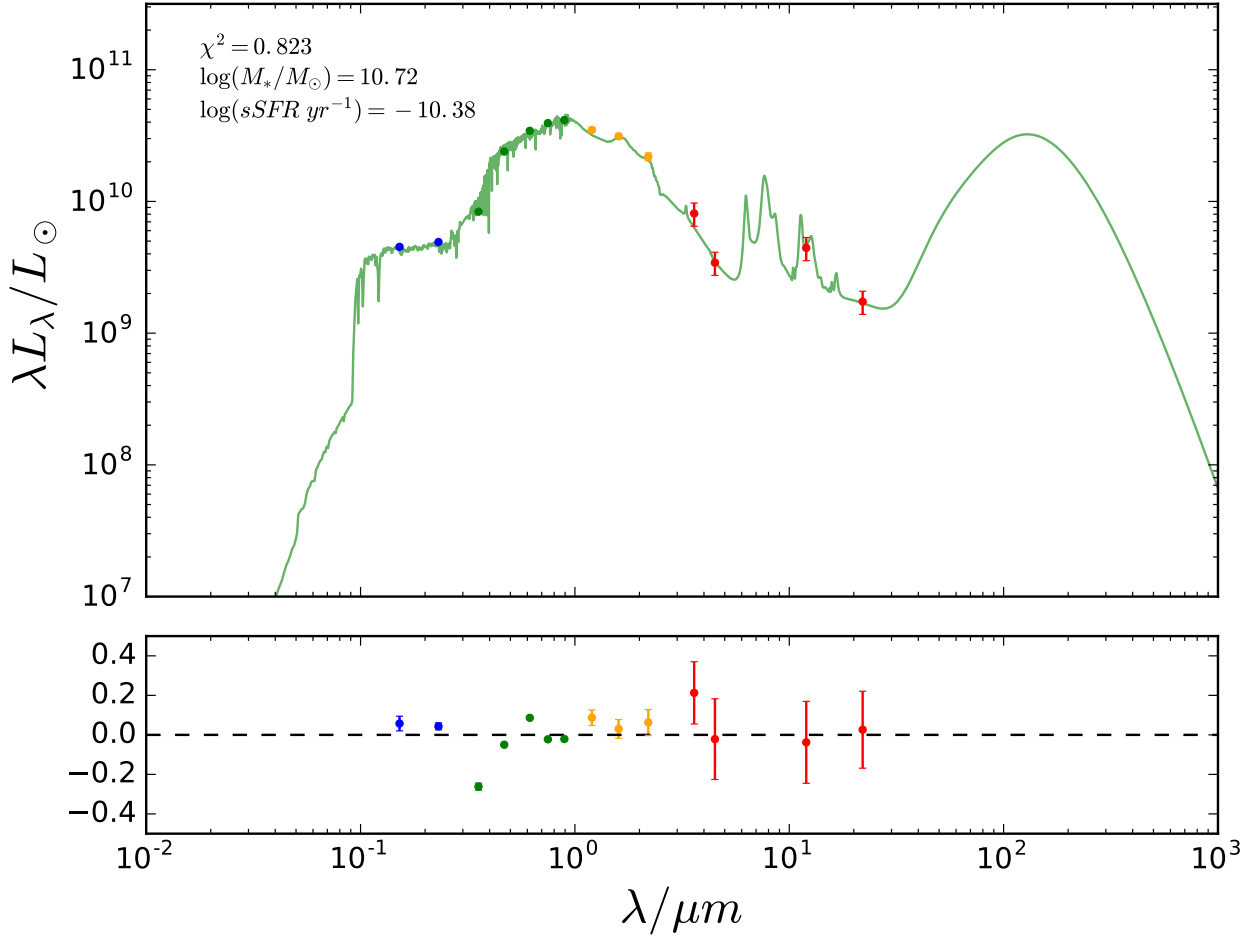


Figure 2. Top panel: shows a typical good fit SED in our sample. The x-axis is the rest frame wavelength and y-axis is the luminosity in solar units. The dots are the observed fluxes in 14 bands from GALEX FUV and NUV (blue), SDSS u, g, r, i, z (green), 2MASS J,H,K (yellow) and the four WISE bands (red). GALEX, SDSS, and 2MASS points show 1σ errors calculated using the magnitude errors from the corresponding catalogs. The four WISE bands have errors of 20%. The green line shows the best fit SED. Bottom panel: The dots show the fractional residues $(L_{\text{true}} - L_{\text{MAGPHYS}})/L_{\text{MAGPHYS}}$. The colour code is same as the top panel. Notice that the PAH emission around $10\ \mu\text{m}$ is not well constrained due to the sparse sampling in this region. Similarly, the dust emission peak around $100\ \mu\text{m}$ is not well constrained due to lack of far infrared observations.

bar. The typical uncertainty in $\log M_*$ is about 0.048 dex, and in $\log \text{sSFR}$ is about 0.125 dex.

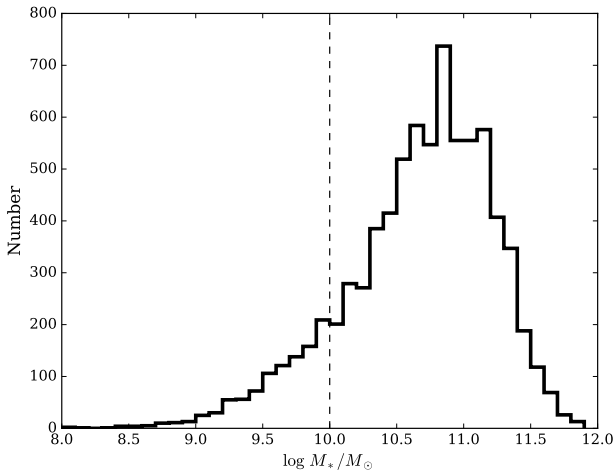
Following Salim (2014), galaxies above the upper green line ($\log \text{sSFR} = -10.8$) are termed as star forming galaxies (SFGs), and those lying under the lower green line ($\log \text{sSFR} = -11.8$) are termed as quenched galaxies (QGs). The region between the horizontal green lines in Figure 6 defines the green valley. We clearly find a bi-modality in the distribution of sSFR also previously noticed in the literature (Brinchmann et al. 2004; Salim et al. 2007; Peng et al. 2010; Weinmann et al. 2006; Wetzel et al. 2012).

We then separate our sample by morphology in to four groups: late-type spirals (LTS), early-type spirals (ETS), S0s, and Ellipticals (Es). In LTS, we group together Sc, Scd, and Sd morphologies, and in ETS we group together Sa, Sab, Sb, and Sbc morphologies. We then plot each of

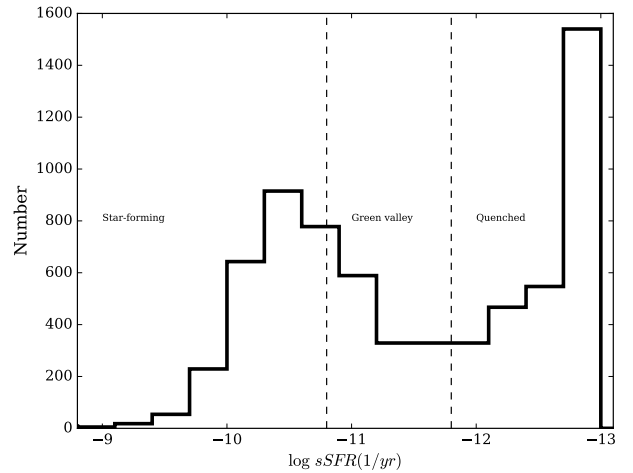
these groups separately on the $\text{sSFR}-M_*$ plot as shown in right panel of Figure 6 in shades of blue. In this figure, the $1/V_{\text{max}}$ -corrected density map shows the position of a particular group on the $\text{sSFR}-M_*$ plane and the contours are repeated for the full sample from the left panel of Figure 6. The region between the green lines is the green valley. The star forming sequence is populated mostly by LTS at the low mass end ($\log M_*/M_\odot \leq 10.5$) and by the ETS at the high mass end. ETS with high mass are also present in the green valley and in the quenched region. Es and S0s populate the region defined for quenched galaxies in the $\text{sSFR}-M_*$ plane with the S0s having a tail in the green valley. Table 3 shows the percentage of galaxies of a given morphology in the star-forming, green valley and quenched regions. As expected, the star-forming region contains a very small number of Es (0.3%) and a small number of S0s (11.8%). ETS, comprising

Table 2. A part of the catalogue of the MAGPHYS output parameters and NA10 morphologies and environmental density for each galaxy in our sample. The full catalogue is available in the electronic version of this paper.

ObjID	R.A. J2000 (deg)	Decl. J2000 (deg)	z	$\log M_*$ (M_\odot)	$\log sSFR$ yr^{-1}	TT	$\log \Sigma$ (Mpc^2)	χ^2
J152757.03+032226.92	231.988	3.37414	0.085	11.71	-12.72	-5	1.199	3.078
J152926.94+032851.96	232.362	3.4811	0.037	10.69	-12.67	-2	0.611	1.239
J094953.04+001854.14	147.471	0.315039	0.064	11.2	-10.62	4	-0.507	2.568
J014921.15+124254.20	27.3381	12.7151	0.034	10.45	-10.32	5	-0.75	0.847
J083114.52+524225.06	127.811	52.707	0.064	11.03	-10.57	2	-0.699	0.554
J085534.67+561207.52	133.894	56.2021	0.045	11.04	-12.97	-2	-0.349	2.461
J084714.08+012144.64	131.809	1.3624	0.04	10.9	-12.17	-5	-0.625	0.818
J120120.28+023125.91	180.335	2.52386	0.021	9.852	-10.52	1	-0.236	1.022
J142720.13+025018.20	216.834	2.83839	0.027	10.54	-10.27	5	-0.13	0.232
J092122.09+545154.28	140.342	54.8651	0.045	11.23	-12.82	-5	0.901	2.485

**Figure 3.** Histogram of stellar mass derived using SED fitting from MAGPHYS. In the final sample only galaxies with $\log M_*/M_\odot \geq 10$ are included.

Sa, Sab, Sb, and Sbc morphologies, constitute 67.1% and LTS constitute 20.1% of the galaxies in the star-forming region. Thus, in the local Universe majority of the recent star formation in massive galaxies happens in ETS and LTS. On the other hand, the quenched region predominantly contains Es (46.2%) and S0s (42.1%) with a small contribution from ETS (11.7%) and almost no contribution from LTS. In the green valley, majority is populated by ETS (49.1%) and S0s (39.9%) and a small percent are Es (8.3%) and LTS (2.7%). Bouquin et al. (2015) also found that in the green valley, defined using GALEX data, S0-Sa galaxies are more common. We find that, in the local Universe, massive galaxies in the green valley are predominantly disk galaxies with a prominent bulge. Further, similar results were also seen from the Galaxy Zoo (GZ) project by Schawinski et al. (2014) which identified galaxies as only early-types and late-types. Since we have detailed morphological classification, we can have a

**Figure 4.** Histogram of sSFR, obtained by dividing the SFR with the stellar mass for each galaxy (note that the x-axis is inverted), showing a bi-modal distribution. We define the star-forming region ($\log sSFR \geq -10.8$), green valley ($-10.8 < \log sSFR < -11.8$), and quenched region ($\log sSFR \leq -11.8$) following Salim (2014).

closer look at the morphology of galaxies undergoing quenching. In particular, a comparison of Fig. 6 with (Schawinski et al. 2014, see Fig. 3) shows that for massive galaxies, most of the GZ late-type galaxies in the green valley and quenched region are likely to have Sa-Sb morphologies. The small number of GZ early-type galaxies in the green valley are mostly S0 galaxies.

In Figure 7, we split the ETS into their morphological subtypes to explore their distribution on the sSFR- M_* plane. We can see that as the bulge becomes more prominent when we move along Sbc to Sa morphology, galaxies gradually make a transition to the quenched region through the green valley. Table 3 also shows that the star-forming region comprises higher percentage of Sbc and Sb galaxies

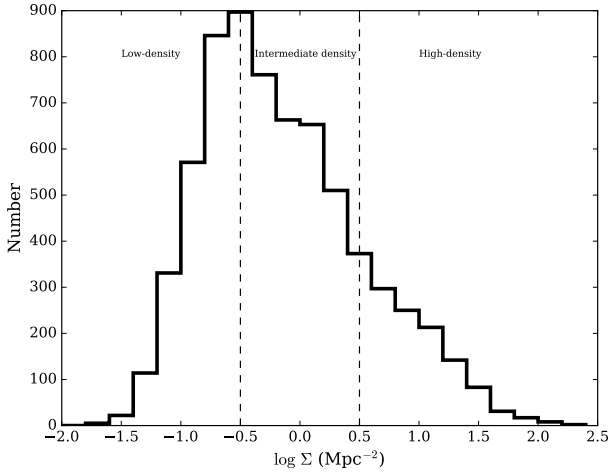


Figure 5. Histogram of local environmental density ($\log \Sigma$ (Mpc^{-2})) for our final sample of galaxies. The dashed lines separate the sample into low, intermediate, and high densities.

Table 3. Morphological fraction of galaxies which are in star-forming, green valley and quenched regions.

	Star-forming	Green-valley	Quenched
Total No.	2184	1288	2789
Es	0.3%	8.3%	46.2%
S0s	11.8%	39.9%	42.1%
Sa	10.7%	18.4%	7.8%
Sab	11.0%	11.2%	1.3%
Sb	26.8%	15.1%	2.3%
Sbc	18.6%	4.4%	0.3%
Sc-Sd	20.8%	2.7%	0.0%

than Sab and Sa. Whereas in the green valley there is a higher percentage of Sa, Sab, and Sb galaxies relative to Sbc galaxies. Also, in the quenched region SAs galaxies are more numerous than Sab, Sb, and Sbc. The main systemic difference between these different subtypes of ETS is in the size and luminosity of the bulge component. The variation we see points towards the importance of the bulge component in the quenching of galaxies. A similar result was also found by [Bluck et al. \(2014\)](#), wherein they found that the bulge mass correlates most with the passive state of a galaxy. [Mendez et al. \(2011\)](#) studied the morphologies of green valley galaxies in the redshift range $0.4 < z < 1.2$ and found that 14% are in merger, 51% are late-type galaxies, and 35% are early-type galaxies. Under the simplistic assumption that all of the merging galaxies in that redshift range will eventually transform into early-type galaxies, the fraction of green valley early-type galaxies will increase to 49%, which is very close to the fraction of early-type galaxies (Es and S0s) in the green valley that we find, which is 48.1%. In reality, the

situation may be much more complicated wherein the environment also plays a role in transforming late-type galaxies into early-type galaxies.

3.1.2 Fraction of galaxies of different morphologies at fixed sSFR, and the differential effect of environment

We study the fraction of LTS, ETS, S0s, and Es in bins of \log sSFR (Fig 8). Here again we correct for the Malmquist bias, using the $1/V_{max}$ method, while calculating the fractions. In each of the \log sSFR bin, we find the fraction of each morphological type as follows (cf. [van den Bosch et al. 2008](#), eq. 2):

$$f_{\text{morph}|s\text{SFR}} = \frac{\sum_{i=1}^{i=N_a} w_i}{\sum_{j=1}^{j=N_b} w_j}, \quad (1)$$

where w_i is the weight for each galaxy calculated using $1/V_{max}$. And N_a is the total number of galaxies of a particular morphological type for a given \log sSFR bin. N_b is the total number of galaxies in that \log sSFR bin. In all the sections that follow, all the fractions are $1/V_{max}$ -corrected using this method. The errors on these fractions are calculated using the jackknife technique following the approach described in [van den Bosch et al. \(2008\)](#).

It is interesting to see in Fig. 8 that the trends for different morphological types are quite different. In accord with earlier results, LTS have a higher fraction (~ 0.3) for \log sSFR ~ -10 and there is a sharp decline in the fraction of LTS with decreasing \log sSFR. Meanwhile, the fraction of ETS shows a steep increase as \log sSFR decreases, with a peak at the boundary of the star-forming and green valley regions. This is followed by a sharp decline in the green valley and then settling at about 10% in the quenched region. Such a decline in the ETS and LTS coincides with a sharp increase in the fraction of S0s and Es with decreasing \log sSFR. A simple interpretation is a morphological transformation of LTS and ETS to S0s and Es, which is accompanied by a decline in the sSFR. Our results are in agreement with the GZ based study of galaxy morphology and color ([Skibba et al. 2009](#), see Fig. 5) where they see a correlation between morphology and color such that the likelihood of early-type galaxy increases as the galaxy color becomes redder. We can put a stronger constraint on the morphologies by suggesting that they are ETS transforming in S0 galaxies in the green valley. Several physical processes can lead to such morphological transformations from late-type to early-type galaxies which also quench the star formation in these galaxies (see [Boselli & Gavazzi 2006](#), for a review and the references therein). This has also been observed in high redshift, upto ~ 1 ([Kovač et al. 2010](#)). Interestingly, there are also two distinct class of S0s galaxies: one which is in the green valley and quenched region and thus hosting an older stellar population, and the other which is actively forming stars (with \log sSFR in the range $[-9, -8]$) hosting a younger stellar population. The latter class of S0s are almost as abundant as the LTS in that \log sSFR bin. [Barway et al. \(2013\)](#) have found similar populations of young and old S0s using UV-near IR colours of galaxies. [Johnston et al. \(2014\)](#) have found S0s in clusters with a younger bulge thus proposing that the final

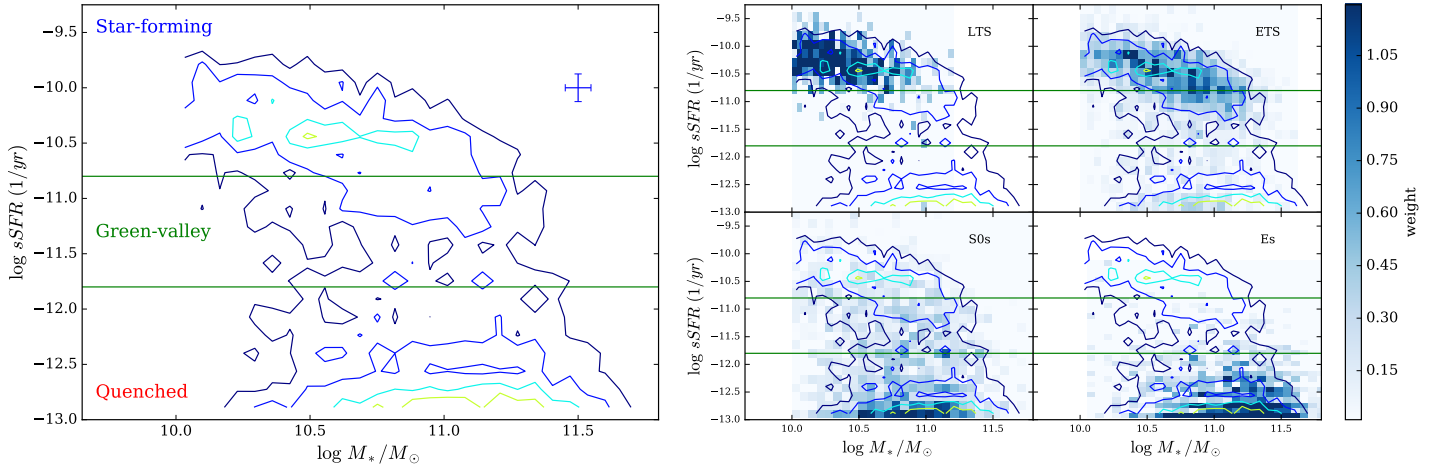


Figure 6. Left Panel: Dependence of specific star formation rate on stellar mass for our entire sample. The contours show the $1/V_{max}$ -corrected density of galaxies on the stellar mass and sSFR plane. The errorbars on the top-right corner show the typical uncertainties in the estimating the stellar mass and sSFR from MAGPHYS. The region between the horizontal green lines defines the green valley from Salim (2014). Galaxies above the upper green line ($\log sSFR = -10.8$) are termed as star forming, and those lying under the lower green line ($\log sSFR = -11.8$) are termed as quenched galaxies. This shows the star-forming main sequence of galaxies, the quenched region at $\log M_*/M_\odot \geq 10.5$, and a well separated transition zone (green-valley) between the two populations. Right Panel: Same as the left-panel after splitting our whole sample, where top left: LTS, top right: ETS, bottom-left: S0s, bottom-right: Es. The shading in blue shows the $1/V_{max}$ -corrected density of galaxies in each morphological class. The contours are from the left panel for the full sample. We see a morphological dependence of the distribution of galaxies on sSFR- M_* plane where the LTS are in the lower mass end ($\log M_*/M_\odot \leq 10.5$) star-forming sequence, ETS are in the high mass end of the star-forming sequence and near the green valley, S0s have a large population in the quenched region and a tail in the green valley, and the Es are mostly quenched.

episode of star formation might be happening in the central regions of cluster S0s.

Some of the physical processes which lead to changes in the star formation and morphologies of galaxies are thought to depend on environment which hosts these galaxies, e.g. ram-pressure stripping (Gunn & Gott 1972), galaxy harassment (Farouki & Shapiro 1981; Moore et al. 1996), and strangulation (Larson et al. 1980). Hence, we need to study the impact of the environment on the relation between morphology and sSFR.

To do this, we split our sample into low density ($\log \Sigma \leq -0.5$), intermediate ($-0.5 < \log \Sigma < 0.5$) density, and high density ($\log \Sigma \geq 0.5$) environments and study the fraction of different morphologies as a function of $\log sSFR$ (Fig. 9). We notice that environmental density does not significantly alter the fraction of individual morphologies as a function of $\log sSFR$, except for Es, which are more abundant in intermediate and high density environments. This is a manifestation of the morphology-density relation (Dressler 1980). The two populations of S0s seen in Figure 8 continue to be present in all the three environments. S0s in green valley and the quenched region show similar trends in all density environments, albeit with large uncertainties.

This result, along with our analysis presented in Section 3.4, indicates that morphology is strongly correlated with sSFR, independent of the environment.

3.1.3 Fraction of star-forming, green valley, and quenched galaxies at fixed morphological T-type, and the differential effect of environment

We divide our whole sample of galaxies into three parts as star-forming ($\log sSFR \geq -10.8$), green valley ($-10.8 > \log sSFR > -11.8$) and quenched ($\log sSFR \leq -11.8$). We then plot the $1/V_{max}$ -corrected fraction of galaxies in each of these types for a fixed morphological T-type (Fig. 10) using the same method illustrated in the earlier sub-section. As we use all the morphological subtypes in this section, we have S0s in three stages: S0- (S0s with a smooth light profile), S0 (S0s with some structure in their light profile), and S0/a (S0s in a transition from Sa spirals). Spiral galaxies range from Sa to Sd.

The overall trend seen in Figure 10, that as we go from early-type to late-type galaxies the quenched fraction decreases, is well expected. However, it is interesting to see that some of the Es are in the green valley (7.9%), and a negligible fraction of them are star-forming (0.4%). These Es may have recently undergone gas-rich minor/major merger which leads to triggering of star-formation in these galaxies. About 70% of the S0- and 65% of the S0 galaxies are quenched. Thereafter, there is a rapid fall in the fraction of quenched S0/a galaxies (and hence a corresponding increase in the star-forming and green valley S0/a). Further, the quenched fraction of Sa spirals only slightly decreases, and interestingly it is almost equal to both the fraction of green valley and star-forming Sa spirals. Spirals from Sab to Sd show a rapid decline in the quenched fraction and green valley. These fractions in terms of percentages are summarized in Table 4.

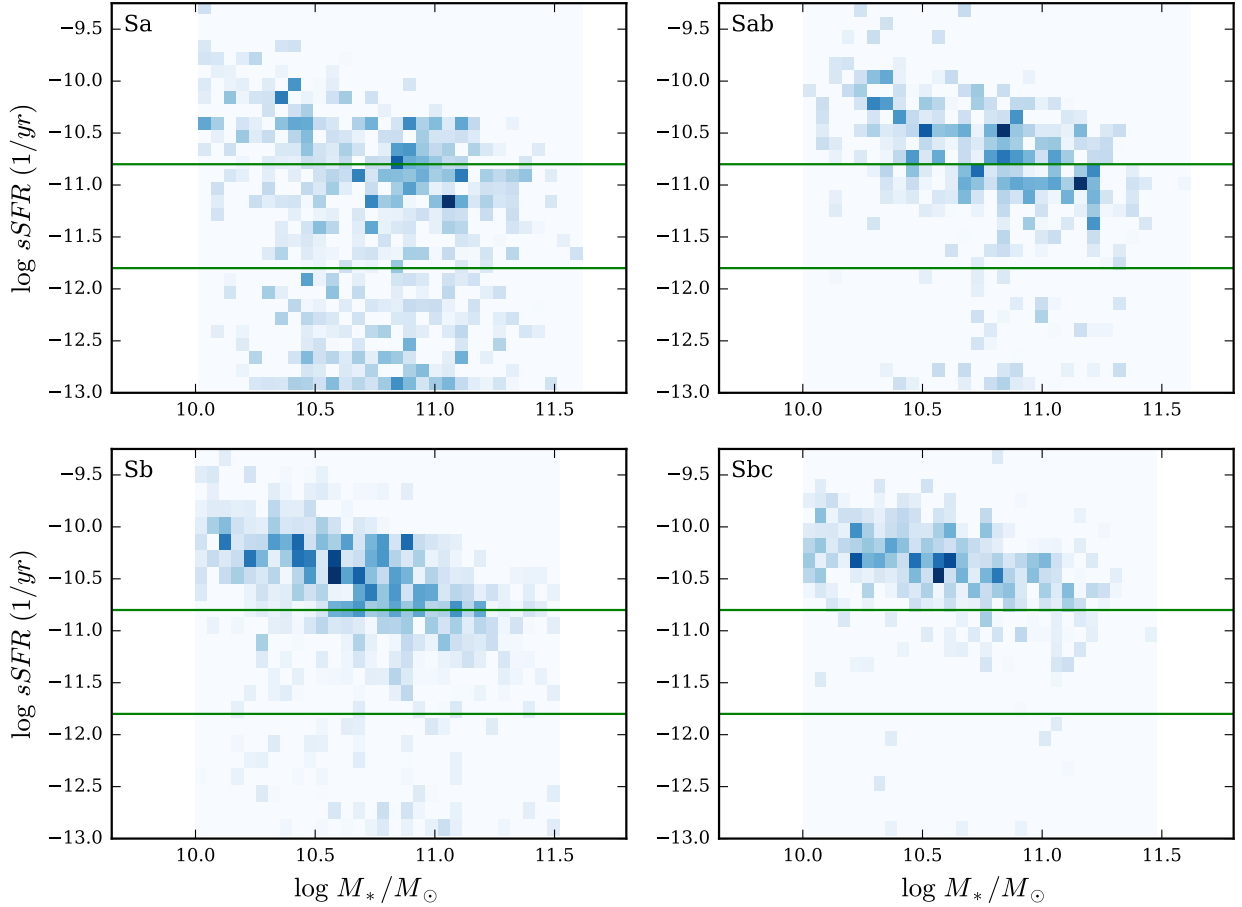


Figure 7. Dependence of specific star formation rate on stellar mass for ETS further split into more detailed morphologies. The region between the horizontal green lines is the green valley. The density map shows the location of galaxies with different morphologies. Top left: Sa spirals, Top right: Sab spirals, Bottom-left: Sb, Bottom-right: Sbc. As we move along the Hubble sequence from Sa to Sbc, galaxies move from the quenched region through the green valley to the star-forming region.

Table 4. Fraction of star-forming, green valley, and quenched galaxies each morphological type.

	E	S0	Sa	Sab	Sb	Sbc	Sc-Sd
Total No. of galaxies	1478	1787	671	429	846	502	548
Star forming galaxies	0.4%	13.5%	34.1%	56.9%	69.6%	86.1%	92.5%
Green valley galaxies	7.9%	26.9%	34.8%	34.4%	23.2%	12.1%	7.2%
Quiescent galaxies	91.7 %	59.6%	31.1%	8.7%	7.2%	1.8%	0.3%

We also examine the role of environment in the quenched fraction of a fixed morphological type. We plot the fraction of star-forming, green valley, and quenched galaxies for a fixed morphological T-type in three different panels. In each panel, we further split in terms of three environmental bins: low, intermediate, and high density (Fig 11). The quenched fraction of Es in all the three environments remains high and almost the same with a small fraction of them in the green valley. LTS (Sc-Sd) remain mostly star forming in all environments.

Interestingly, quenched ETS are present in all environments and their quenched fraction increases with increasing

environment density. The strongest effect of environment is seen on the Sa spirals and S0/a galaxies, wherein their quenched fraction increases with increasing environmental density. Note that the fraction of quenched Sa spirals which is around 30% in low and intermediate density environments, suddenly rises to about 50% in the high density environment. This shows that environment does play a role in quenching of Sa spirals, however the physical process of quenching is likely to be gentle since their spiral arms are intact. This rules out ram-pressure stripping for the quenching of these galaxies, and makes a gentler process like strangulation more likely. Our results are in agreement with those of [van den Bosch](#)

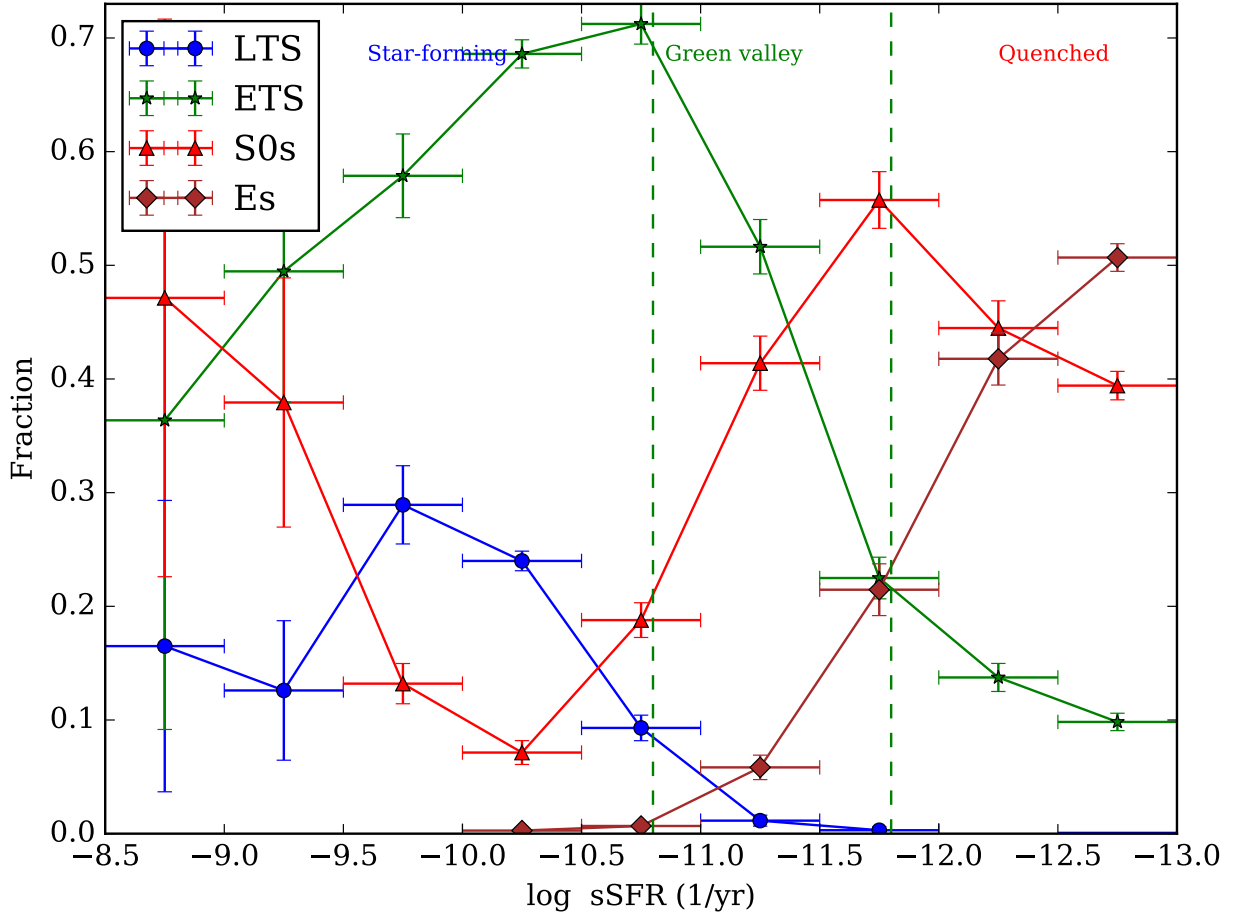


Figure 8. Fraction of galaxies of different morphological type (LTS in blue, ETS in green, S0s in red, and Es in brown) as a function of log sSFR. The errorbars are jackknife errors. Fraction of LTS and ETS decline with decreasing log sSFR, which coincides with an increase in the fraction of S0s and Es. S0s on the other hand also show a second population, which is actively forming stars. See text for a detailed discussion.

et al. (2008) and Peng et al. (2015), where the authors argue for strangulation as the dominant quenching mechanism in local galaxies.

The quenched fraction of S0/a galaxies, which are in transition from Sa to S0, also increases with increasing environmental density. S0- and S0 are mostly quenched in all environments with their fraction increasing by about 10% in high density environment. The abundance of quenched S0- and S0 in intermediate and particularly in low density environments is intriguing. According to Baldry et al. (2006) (see their Fig. 9 caption), $\log \Sigma > 0.8 \text{ Mpc}^{-2}$ corresponds to cluster like environments. Thus, our definition of low and intermediate densities, $\log \Sigma < 0.5 \text{ Mpc}^{-2}$, will correspond to field and group like environment. Thus, at low densities, ram-pressure stripping may not be a dominant mechanism in the formation of S0 galaxies. Interestingly, in low density environments about 30% of the S0/a galaxies are star-forming. Even though this fraction decreases with increasing density, in intermediate and high densities about 20% and 10% of

the S0/a galaxies are star-forming, respectively. About 10% of the S0 and S0- are star-forming in the low density environment, and their fraction decreases when we go to the high density environment. The presence of such star-forming S0s in all environments gives rise to the second population of star-forming S0s previously seen in Figure 9.

Thus, we conclude that for massive galaxies in the local Universe, only the quenched fraction of S0/a and S0 galaxies show a significant dependence on environmental density. Further, the fact that the quenched fraction of S0/a galaxies is more close to that of Sa spirals and much lower than that of S0 and S0-, shows that S0/a galaxies likely undergo a different quenching process than that of S0 and S0- galaxies.

3.2 Relation between morphology and local environment

Next we study the dependence of morphology on the local environmental density. We follow a similar procedure as in

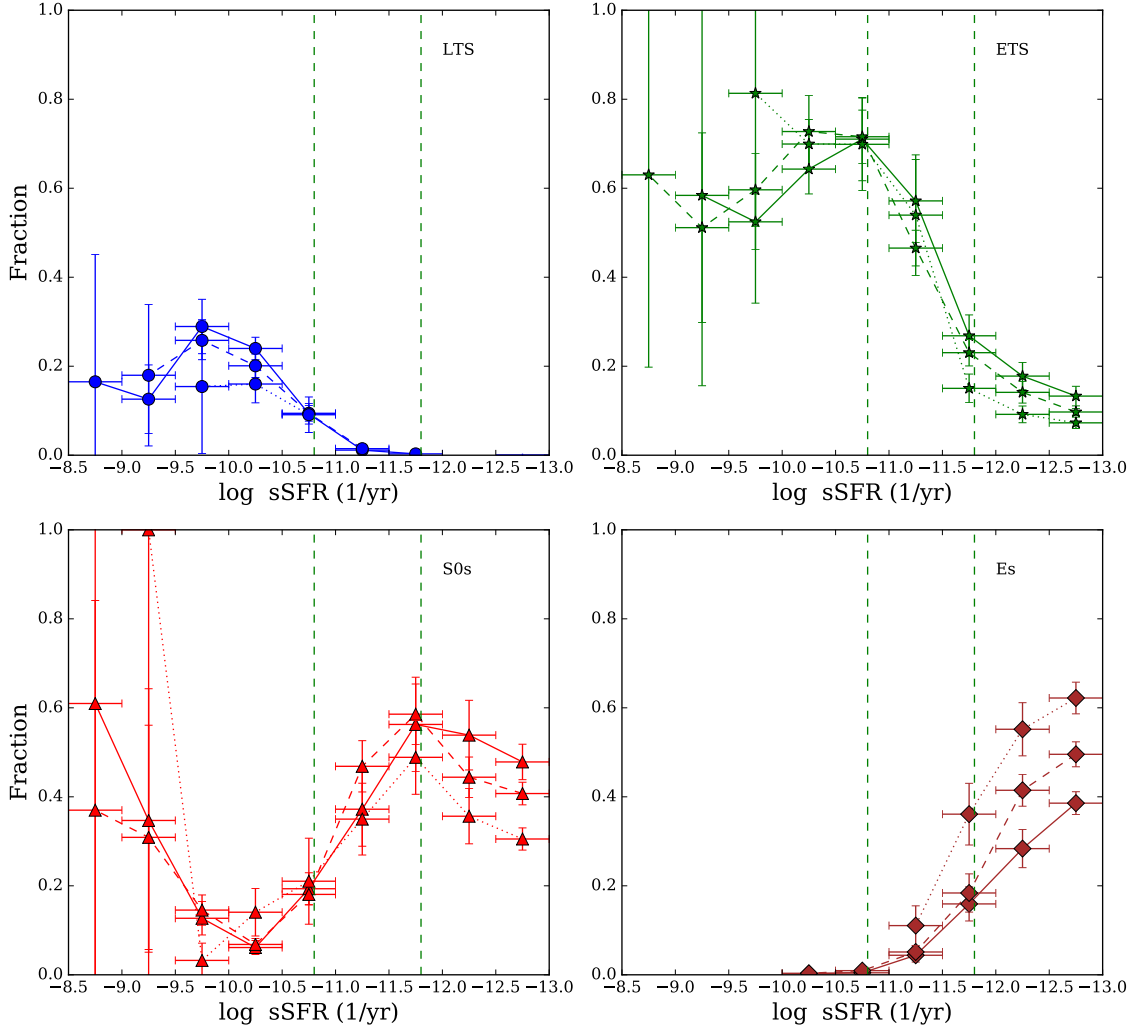


Figure 9. Fraction of galaxies of different morphological type (the colour code is same as Fig. 8) in each panel. And in each panel we further split with environmental density in terms of low density ($\log \Sigma \leq -0.5$)-filled line, intermediate ($-0.5 < \log \Sigma < 0.5$)-dashed line, and high density ($\log \Sigma \geq 0.5$)-dotted line. The errorbars are jackknife errors. Notice that fraction of ETS at fixed $\log \text{sSFR}$ does not change significantly with environment. Es are more abundant in intermediate and high densities. LTS are more abundant in low and intermediate densities. There continue to be two populations of S0s (green valley/quenched S0s and star forming S0s) in all environments.

Section 3.1. We first examine the fraction of galaxies with different morphologies in fixed environmental bins. We then study the differential effect of sSFR on this relation.

In Figure 12, we plot the the $1/V_{max}$ -corrected fraction of Es, S0s, ETS, and LTS galaxies in fixed environmental bins. In high density environments ($\log \Sigma > 0.5$) the fraction of ETS decreases and the fraction of Es increases. This is the well known morphology-density relation (Dressler 1980). Interestingly, the fraction of S0s does not increase as we go to high densities. One reason might be that we only have massive galaxies in our sample, and the effects of environment (e.g. ram-pressure stripping), which can transform a spiral into an S0, is stronger for low-mass galaxies (Mori & Burkert 2000; Marcolini et al. 2003; Bekki 2009; Fillingham et al. 2016; Emerick et al. 2016). LTS are most abundant in very low densities ($\log \Sigma \sim -1.5$) and gradually decline with increasing environmental density. The morphological fraction of galaxies split in three environmental bins: low-density, in-

termediate density, and high density is summarised in Table 5.

We split our sample into star-forming, green valley, and quenched galaxies and plot the fraction of galaxies with different morphologies in fixed environmental bins (Fig. 13). Notice that the morphology-density relation does change, this is partly because of the paucity of star-forming Es and quenched/green valley LTS. In the left panel of Fig. 13, fraction of star-forming LTS gradually declines with increasing environment and the fraction of star-forming ETS increases, although within errorbars it is not very significant. Except that in the highest density bin ($1.5 < \log \Sigma \leq 2.0$) the trend is reversed; however this feature is not very significant due to the large errorbars. Interestingly, in all environments, except in the lowest density bin, about 10% of the star-forming galaxies are S0s. These are the second population of actively star-forming S0s observed in Figure 9. The ubiquity of these S0s in all environments, from low density to high density

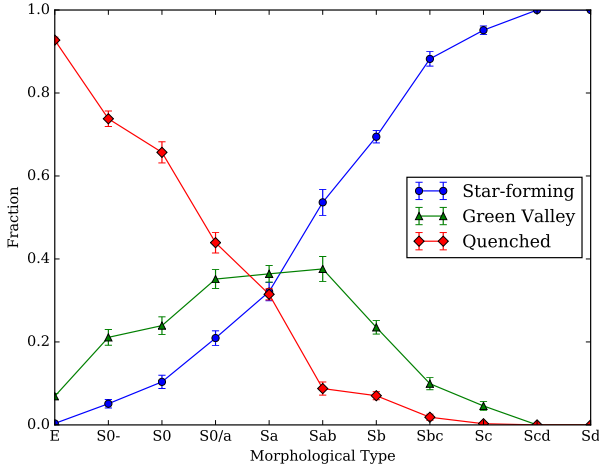


Figure 10. Fraction of star-forming (blue), green valley (green) and quenched (red) galaxies for a fixed morphological T-type going to Es to Im spirals. The errorbars are jackknife errors. Notice that the quenched fraction decreases as we move from early-type galaxies to late-type. The fraction of green valley galaxies increases from Es to S0s and upto Sab spirals beyond which there is a steep decline. Interestingly Sa spirals shows equal fractions of all three stages of star-formation.

Table 5. Fraction of galaxies of different morphological types in low, intermediate, and high density environments.

	Low density	Intermediate density	High density
Total No.	2158	2968	1135
Es	12.0%	21.4%	42.7%
S0s	29.2%	31.9%	31.4%
Sa	13.4%	10.9%	7.1%
Sab	7.9%	6.9%	4.5%
Sb	15.7%	14.1%	8.4%
Sbc	9.4%	7.9%	3.5%
Sc-Sd	12.4%	6.9%	2.4%

requires further study. In all environments, the green valley galaxies (middle panel of Fig. 13) are mostly ETS (around 50%) and S0s (around 40%), except in the highest density bins which show a decline. The fraction of green valley Es increases with increasing density with a steep rise in the highest density bin, wherein around 75% of the green valley galaxies are Es. These might be Es which have undergone recent gas rich minor/major merger(s). Since the rate of merger increases with increasing environmental density we find more Es in green valley in such environments. For quenched galaxies (right most panel of Fig. 13), the fraction of Es increase with increasing environmental density which most likely arises from the morphology-density relation. Except in the lowest density bin, the fraction of quenched S0s

show a weak decline with increasing density, which is possibly because of the increase in the fraction of Es. The fraction of ETS declines very rapidly from the lowest density bin towards intermediate densities and then remains constant at around 10% with a small decline in the highest density bin. Interestingly, in the lowest density bin ($\log \Sigma < -1.5$) there are no quenched S0s, and about 80% of the galaxies are ETS and about 20% are Es.

We examine the percentage of Es, S0s, ETS, and LTS in low, intermediate, and high densities as shown in Table 6. Surprisingly, most of the Es, S0s, and ETS are present in the intermediate density environment.

3.3 Relation between specific star formation rate and local environment

We now study the relation between the two remaining parameters, sSFR and environment. We follow a similar procedure as in the earlier two subsections. We first examine the fraction of star-forming, green valley and quenched galaxies for fixed environmental bins. Then we use the morphological classification in terms of LTS, ETS, S0s and Es to study the differential effect of morphology on the relation between sSFR and environment.

The $1/V_{max}$ -corrected fraction of star-forming, green valley, and quenched galaxies in fixed environmental bins is shown in Figure 14. The quenched fraction increases with increasing environmental density (and hence the star-forming fraction decreases). Interestingly, the fraction of green valley galaxies remains almost constant at about 20% in all environments, except in the lowest and highest environment bin where there is a small decline in the fraction of green valley galaxies. This was also observed by [Wetzel et al. \(2012\)](#) for the green valley defined using $H\alpha$ based SFRs. In Table 7, we summarise the percentage of star forming, green valley, and quenched galaxies in low, intermediate, and high density environments where we observe the same trend as in Figure 14. This shows a strong effect of environment in quenching of galaxies.

The fraction of star-forming, green valley, and quenched galaxies for fixed environmental bins, separately for LTS, ETS, S0s, and Es is shown in Figure 15. We see that most of the LTS are star-forming and most of the Es are quenched in all environments. About 10% of all the Es are in the green-valley in all environments. Star-forming ETS decrease with increasing environmental density, which will get quenched and hence the quenched fraction will increase. Some of them may also transform into quenched S0s which is seen as an increase in the quenched fraction of S0s. Interestingly, S0s in lowest environmental density bin are mostly star-forming (the exact fraction however has very large uncertainty) and there are no green valley, and quenched S0s. Further, the fraction of star-forming and green valley S0s show a gradual decline with increasing environmental density.

Finally, we report the percentage of galaxies in low density, intermediate density, and high density environments which are in the star-forming, green valley, and quenched region in Table 8. As expected, the percentage of star-forming galaxies is highest at low/intermediate densities and drastically decreases at high densities. The percentage of green valley galaxies increases from low to intermediate densities and then shows a significant decrease at high densities. The

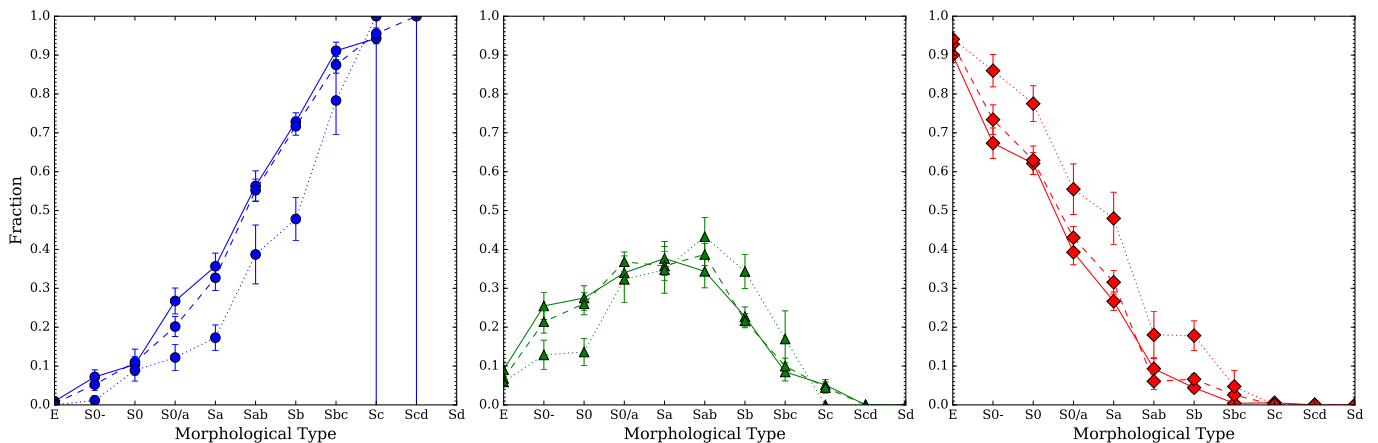


Figure 11. Fraction of star-forming (blue), green valley (green) and quenched (red) galaxies for a fixed morphological T-type shown in the left, middle, and right panel respectively. In each panel we further split in three environmental bins: low density ($\log \Sigma \leq -0.5$)-filled line, intermediate ($-0.5 < \log \Sigma < 0.5$) density-dashed line, and high density ($\log \Sigma \geq 0.5$)-dotted line. The errorbars are jackknife errors. Notice that in all environments as we go from early-type galaxies to late-type the quenched fraction decreases. However, the effect of environment on quenching is most apparent on Sa and S0s, wherein their quenched fraction increases substantially in high density environments. Interestingly, in low density environments the fraction of star-forming S0/a galaxies is high.

Table 6. Fraction of galaxies in low, intermediate, and high densities for different morphological types.

	E	S0	Sa	Sab	Sb	Sbc	Sc-Sd
Total No. of galaxies	1478	1787	671	429	846	502	548
Low density	18.2%	31.8%	40.8%	38.9%	38.8%	41.3%	52.7%
Intermediate density	46.8%	48.3%	47.6%	49.0%	50.0%	50.3%	41.8%
High density	35.0%	18.4%	11.6%	12.1%	11.2%	8.4%	5.5%

Table 7. Fraction of star-forming, green valley, and quenched galaxies in low, intermediate, and high densities.

	Low density	Intermediate density	High density
Total No.	2158	2968	1135
Star forming	46.1%	35.1%	15.6%
Green valley	21.9%	21.6%	17.3%
Quenched	32.0%	43.3%	67.1%

Table 8. Fraction of galaxies in low, intermediate, and high densities which are in star-forming, in green valley, and in the quenched regions.

	Star forming	Green valley	Quenched
Total No.	2184	1288	2789
Low density	44.0%	35.1%	24.6%
Intermediate density	48.0%	49.9%	47.7%
High density	8.0%	15.0%	27.7%

percentage of quenched galaxies increases from low to intermediate densities and then decreases at high densities.

3.4 Partial correlation coefficient between morphological T-type, sSFR, and Σ

In the previous sections, we studied the relation between each of the three parameters, morphology, sSFR, and environment, taken two at a time, and then studied the differential effect of the third parameter. In this section, we quantify these relations using the partial correlation coefficient (PCC).

The PCC measures the correlation between any two variables by removing the effect of a set of control variables.

For instance, in our study we know that morphological T-type and \log sSFR are correlated (as the T-type increases \log sSFR increases). However, we know that T-Type and environmental density (Σ) is anti-correlated because of the morphology-density relation (as Σ increases the fraction of early-type galaxies increases i.e. T-type decreases). And Σ and \log sSFR are also anti-correlated, since as Σ increases, \log sSFR decreases. Thus, it is possible that the correlation between morphology and \log sSFR is caused by the effect of environment. In other words, because it is more likely to find early-type galaxies in high density environments, and because high density environments are more efficient at quenching galaxies, we find that early-type galax-

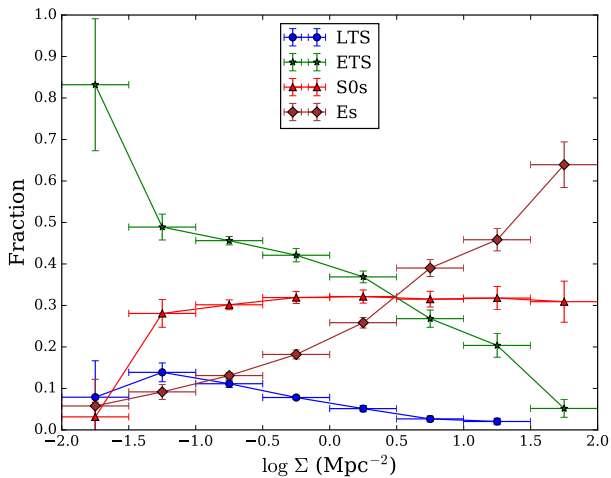


Figure 12. Fraction of LTS (blue), ETS (green), S0s (red), and Es (brown) in fixed environmental bins. The errors shown are jackknife errors. Notice the fraction of ETS decreases, and the fraction of Es increases in the high density environments.

Table 9. Results from the partial correlation coefficient analysis. The errors on the correlation coefficients are calculated using the jackknife method.

Variables (control variable)	Spearman's ρ	PCC
T-type-log sSFR (Σ)	0.752 ± 0.003	0.735 ± 0.003
T-type- Σ (log sSFR)	-0.256 ± 0.010	-0.099 ± 0.011
Σ -log sSFR (T-type)	-0.256 ± 0.010	-0.100 ± 0.010

ies are mostly quenched. Similarly, it is possible that we see a morphology-density relation because as the density increases quenching becomes more efficient, and hence the log sSFR decreases, and because low levels of log sSFR is found mainly in early-type galaxies, we see an anti-correlation between morphology and density. A similar case can be made of the other two variables.

Thus, we find the PCC between: morphological T-type-log sSFR with Σ as the control variable, morphological T-type- Σ with log sSFR as the control variable, and log sSFR- Σ with morphological T-type as the control variable for our final sample of 7079 galaxies.

The PCC between any two random variables A and B with C as the control variable is calculated using,

$$\rho_{AB-C} = \frac{\rho_{AB} - \rho_{AC}\rho_{CB}}{\sqrt{1 - \rho_{AC}^2}\sqrt{1 - \rho_{CB}^2}}, \quad (2)$$

where ρ_{AB} is the Spearman's rank correlation coefficient between the variables A and B.

The results of our PCC analysis are given in Table 9, for reference we also show the Spearman's rank correlation coefficient (Spearman's ρ). Since we use 6194 data points for the PCC analysis, our results are highly significant. The Spearman's ρ shows that the correlation between T-type

and log sSFR is high, which remains so even for the PCC. This suggests that morphology correlates very well with log sSFR, independent of the environment. The Spearman's ρ between T-type- Σ , and Σ -log sSFR is weakly anti-correlated, which considerably decreases after computing the PCC.

Thus we find that for massive galaxies, morphology is the strongest indicator of log sSFR, and that such a relationship is real and not just an indirect effect due to the morphology-density relation and density-sSFR relation. This shows that, at least for massive galaxies, the physical processes which shape the galaxy morphology are also the most important in deciding their star forming state.

4 SUMMARY & CONCLUSIONS

In this work, we have studied the spectral energy distributions of massive galaxies ($\log M_*/M_\odot \geq 10.0$) along the Hubble sequence, from Es to spirals, using multi-wavelength SED fitting using UV-optical-mid IR data from GALEX-SDSS-2MASS-WISE, for a sample of 6194 galaxies. For these galaxies, we are able to simultaneously constrain the recent star formation using UV data and also take into account the dust attenuation from warm dust using IR data. We compute the star formation rate and the stellar mass for each galaxy in our sample using stellar population synthesis models. Further, due to the availability of GALEX UV data, we could define a green valley which has less contamination from the star-forming and quenched region. For our whole sample, the detailed visual morphologies in terms of the Hubble T-types were taken from NA10. Also for our whole sample we had local environmental density from Baldry et al. (2006). Using the morphological classifications, specific star formation, and environmental density information, we studied the mutual dependence of each of these parameters. Our results are summarised as follows:

(i) We find that for massive galaxies in the local Universe, LTS, and Es are primarily star-forming and quenched, respectively. The green valley is mostly populated by ETS (49.1%) and S0s (39.9%). A further split of ETS into Sa, Sab, Sb and Sbc shows that the growth of the bulge plays an important role in quenching. Given that these galaxies are more likely to host a classical bulge which is already quenched, the final process of quenching likely takes place in the disk. The typical quenching timescale of green valley disk galaxies are known to be large, of the order of more than 1 Gyr (Schawinski et al. 2014) and hence the disk quenching must be a slow process (e.g., halo-quenching, strangulation). S0s, on the other hand, which also host a bigger bulge have a disk that may have quenched more rapidly (timescales of less than 250 Myrs) than ETS and hence they are more abundant in the quenched region. The properties of both the ETS and S0s show that at least at the high mass end ($M_{\text{stellar}} > 10^{10} M_\odot$), bulge growth is important for quenching, as was also observed by Bluck et al. (2014).

(ii) The fraction of galaxies of different morphological types (LTS, ETS, S0s and Es) as a function of log sSFR show very different trends. The distribution of LTS peaks at much lower log sSFR and falls quite rapidly for log sSFR > -10 . On the other hand, the fraction of ETS peak near the blue end of the green valley, and falls as we enter the green valley. Interestingly, this fall coincides with the rise

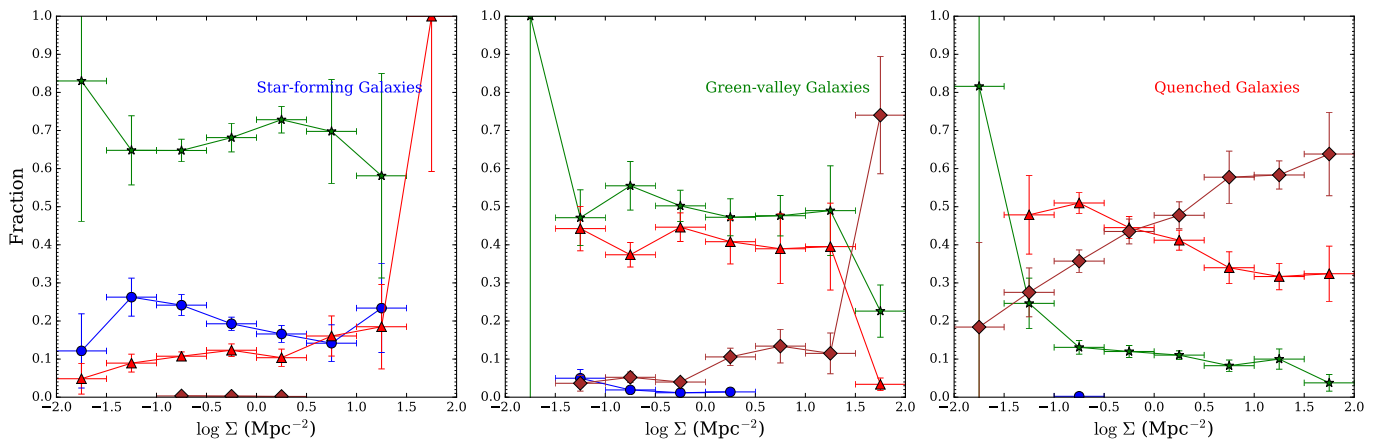


Figure 13. Fraction of LTS (blue), ETS (green), S0s (red), and Es (brown) in fixed environmental bins split in three parts: star-forming galaxies in the left panel, green valley galaxies in the middle panel, and quenched galaxies in the right panel. The errors shown are jackknife errors. Notice the presence of star forming S0s at all environmental densities. ETS and S0s populate the green valley galaxies in all environments, except in the highest environmental density bin. Further, the fraction of green Es increase with increasing environmental density. See the text for a detailed discussion.

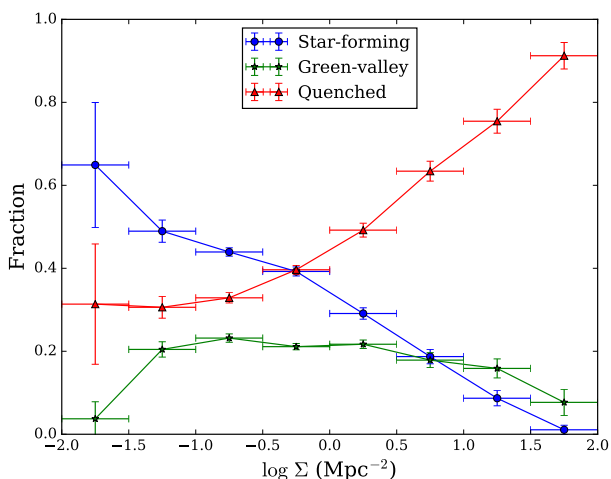


Figure 14. Fraction of star-forming (blue), green valley (green), and quenched (red) galaxies for fixed environmental bins. The errorbars are jackknife errors. Notice that the fraction of star-forming galaxies decreases with increasing environmental density. The fraction of green valley galaxies does not show a significant change with environmental density.

in the fraction of S0s, which peak near the red end of the green valley. This points towards the morphological transformation from ETS to S0s. Beyond the green valley, in the quenched region, the fraction of S0s and ETS declines, and the fraction of Es starts dominating. Interestingly, we also find a second population of S0s galaxies which are actively star forming. A split of our sample into low, intermediate and high densities shows that this relation does not change significantly with environment. Remarkably, even the second population of star forming S0s is present in all the three environmental bins. This supports the view that morphology

is a strong indicator of the sSFR of a galaxy, with a weaker dependence on the environment.

(iii) The fraction of star forming, green valley, and quenched galaxies for a given morphological T-type shows that as we go from Es to late type galaxies, the quenched fraction decreases. As was earlier observed, the fraction of green valley galaxies rises from S0- to Sab galaxies, showing that, in the local Universe, they are the galaxies in transition from star forming to the quenched region. Remarkably, the quenched fraction of S0- and S0 galaxies is much higher compared to the quenched fraction of S0/a galaxies, which is more closer to that of Sa spirals. Furthermore, when we split this relation into low, intermediate and high densities, we find that at low densities, the fraction of star forming S0/a galaxies is higher than the quenched fraction. Further, at high densities there is a rise in the quenched fraction of S0/a galaxies. Also, the quenched/star-forming fraction of S0/a galaxies more closely follows the Sa galaxies in all environments, and unlike the S0- and S0 galaxies, who have a much higher quenched fraction in all environments. This indicates that S0/a galaxies undergo a different quenching process than that of S0-, and S0 galaxies.

(iv) We observe the morphology-density relation for our sample of galaxies, with the exception that the fraction of S0s remain roughly constant as we go to higher densities. This is likely because, we only have high mass S0s in our sample. The split of the morphology-density relation in terms of star-forming, green valley and quenched galaxies shows that there are green valley galaxies in all environments and they are mostly dominated by ETS, and S0s. The fraction of green valley Es rise with increasing environmental density, suggesting that they may have undergone recent gas rich major/minor merger(s). Interestingly, we also see the presence of star forming S0s in all environments, from low to high densities.

(v) The quenched fraction increases with increasing environmental density, and except for the lowest and the highest density bin, the fraction of green valley galaxies remains con-

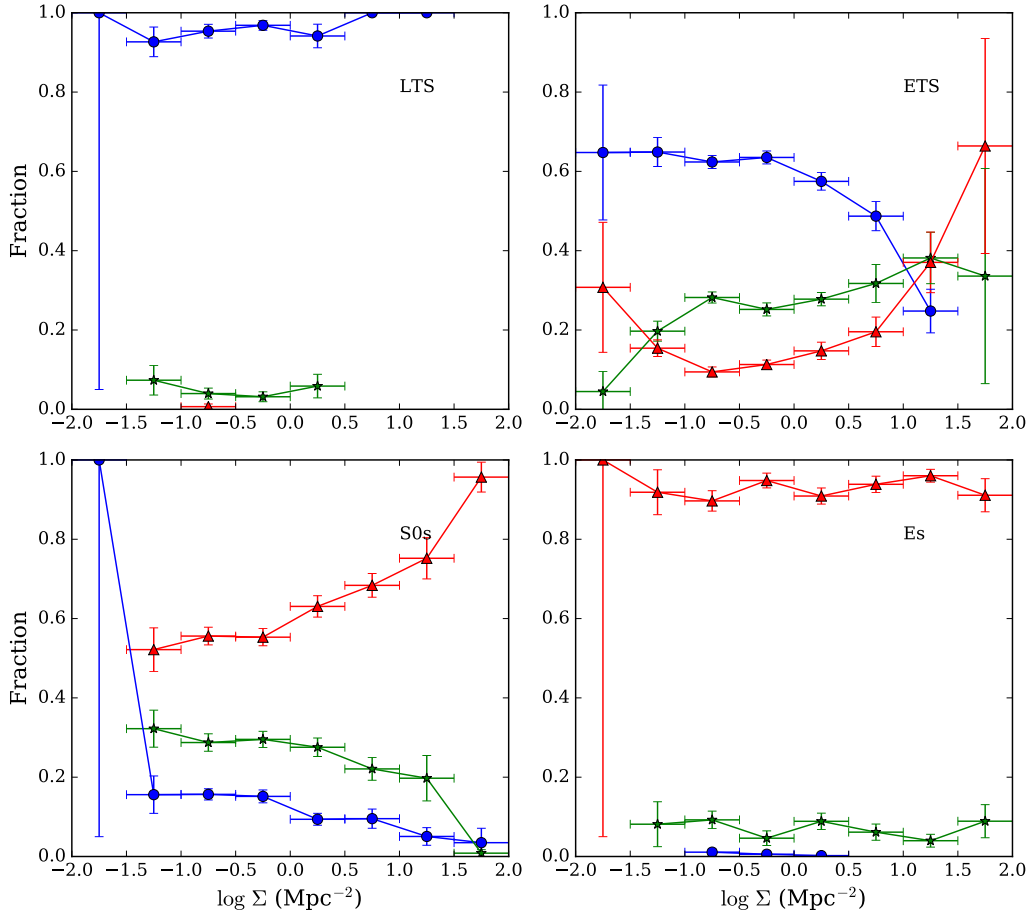


Figure 15. Fraction of star-forming (blue), green valley (green), and quenched (red) galaxies for LTS (top left), ETS (top right), S0s (bottom left), and Es (bottom right). LTS(Es) are star-forming(quenched) as a function of environment. The errorbars are jackknife errors. Star-forming ETS fraction decreases and quenched S0 fraction increases with increasing environmental density.

stant. This shows that, in the local Universe, massive galaxies are recently undergoing transition in all environments. A split of this relation with different morphological class (LTS, ETS, S0s, and Es) shows that ETS and S0s are the galaxies most affected by environment. The fraction of star forming ETS decline with increasing density, some of which move into the green valley and quenched regions. This decline coincides with the increase in the fraction of quenched S0s, showing that possibly some of the quenched ETS also undergo a morphological transformation into S0s. Star forming S0s are most abundant in the lowest density bin, and they decrease as we go to higher densities.

(vi) Because morphology, \log sSFR, and environmental density are correlated with each other, we find the partial correlation coefficient by taking two of the variables with the third variable as the control parameter. Our analysis shows that the correlation between morphology and \log sSFR is strongest, and independent of the environment. Whereas the anti-correlations between morphology-density, and density-sSFR are both weaker when we remove the effect of the third parameter.

In conclusion, we studied the star formation history using multi-wavelength data from UV-optical-mid IR along

the Hubble sequence for a sample of 6194 galaxies. Our results shows that, in the local Universe, for massive galaxies, ETS and S0s are currently undergoing transition from star-forming to the quenched region. There are two populations of S0s, a quenched and an actively star forming one which is present in all environments. Further, our study of morphology, star formation and environment shows that morphological T-type is the strongest indicator of the sSFR of a galaxy independent of the environment. The impact of environment in deciding whether a galaxy is quenched or not, is seen mainly on S0/a, Sa, and Sab type galaxies.

ACKNOWLEDGEMENTS

We thank the anonymous referee for insightful comments that have improved both the content and presentation of this paper. YW thanks IUCAA for hosting him on his sabbatical when the early part of this work was completed. SB would like to acknowledge support from the National Research Foundation research grant (PID-93727). SB, YW and OB acknowledge support from a bilateral grant under the Indo-South Africa Science and Technology Cooperation

(PID-102296) funded by Departments of Science and Technology (DST) of the Indian and South African Governments.

GALEX (Galaxy Evolution Explorer) is a NASA Small Explorer, launched in 2003 April. We gratefully acknowledge NASA's support for construction, operation, and science analysis for the GALEX mission, developed in cooperation with the Centre National d'Études Spatiales of France and the Korean Ministry of Science and Technology.

This research has made use of the NASA/IPAC Extragalactic Database (NED), which is operated by the Jet Propulsion Laboratory, California Institute of Technology (Caltech) under contract with NASA.

Funding for SDSS-III has been provided by the Alfred P. Sloan Foundation, the Participating Institutions, the National Science Foundation, and the U.S. Department of Energy Office of Science. The SDSS-III web site is <http://www.sdss3.org/>.

SDSS-III is managed by the Astrophysical Research Consortium for the Participating Institutions of the SDSS-III Collaboration including the University of Arizona, the Brazilian Participation Group, Brookhaven National Laboratory, University of Cambridge, Carnegie Mellon University, University of Florida, the French Participation Group, the German Participation Group, Harvard University, the Instituto de Astrofísica de Canarias, the Michigan State/Notre Dame/JINA Participation Group, Johns Hopkins University, Lawrence Berkeley National Laboratory, Max Planck Institute for Astrophysics, Max Planck Institute for Extraterrestrial Physics, New Mexico State University, New York University, Ohio State University, Pennsylvania State University, University of Portsmouth, Princeton University, the Spanish Participation Group, University of Tokyo, University of Utah, Vanderbilt University, University of Virginia, University of Washington, and Yale University.

This publication makes use of data products from the Two Micron All Sky Survey, which is a joint project of the University of Massachusetts and the Infrared Processing and Analysis Center/California Institute of Technology, funded by the National Aeronautics and Space Administration and the National Science Foundation. This publication makes use of data products from the Wide-field Infrared Survey Explorer (WISE), which is a joint project of the University of California, Los Angeles, and the Jet Propulsion Laboratory/California Institute of Technology, funded by the National Aeronautics and Space Administration.

REFERENCES

- Alam S., et al., 2015, *ApJS*, **219**, 12
- Baldry I. K., Glazebrook K., Brinkmann J., Ivezić Ž., Lupton R. H., Nichol R. C., Szalay A. S., 2004, *ApJ*, **600**, 681
- Baldry I. K., Balogh M. L., Bower R. G., Glazebrook K., Nichol R. C., Bamford S. P., Budavari T., 2006, *MNRAS*, **373**, 469
- Barway S., Wadadekar Y., Vaghmare K., Kembhavi A. K., 2013, *MNRAS*, **432**, 430
- Bekki K., 2009, *MNRAS*, **399**, 2221
- Bluck A. F. L., Mendel J. T., Ellison S. L., Moreno J., Simard L., Patton D. R., Starkenburg E., 2014, *MNRAS*, **441**, 599
- Boselli A., Gavazzi G., 2006, *PASP*, **118**, 517
- Bouquin A. Y. K., et al., 2015, *ApJ*, **800**, L19
- Brinchmann J., Charlot S., White S. D. M., Tremonti C., Kauffmann G., Heckman T., Brinkmann J., 2004, *MNRAS*, **351**, 1151
- Brown M. J. I., Jarrett T. H., Cluver M. E., 2014, *Publ. Astron. Soc. Australia*, **31**, HASH
- Bruzual G., Charlot S., 2003, *MNRAS*, **344**, 1000
- Charlot S., Fall S. M., 2000, *ApJ*, **539**, 718
- Cheung E., et al., 2012, *ApJ*, **760**, 131
- Croton D. J., et al., 2006, *MNRAS*, **365**, 11
- Daddi E., et al., 2007, *ApJ*, **670**, 156
- Dekel A., Birnboim Y., 2006, *MNRAS*, **368**, 2
- Dressler A., 1980, *ApJ*, **236**, 351
- Elbaz D., et al., 2007, *A&A*, **468**, 33
- Emerick A., Mac Low M.-M., Greevich J., Gatto A., 2016, *ApJ*, **826**, 148
- Fang J. J., Faber S. M., Koo D. C., Dekel A., 2013, *ApJ*, **776**, 63
- Farouki R., Shapiro S. L., 1981, *ApJ*, **243**, 32
- Fillingham S. P., Cooper M. C., Pace A. B., Boylan-Kolchin M., Bullock J. S., Garrison-Kimmel S., Wheeler C., 2016, *MNRAS*, **463**, 1916
- Gunn J. E., Gott III J. R., 1972, *ApJ*, **176**, 1
- Hayward C. C., Smith D. J. B., 2015, *MNRAS*, **446**, 1512
- Hubble E. P., 1926, *ApJ*, **64**
- Johnston E. J., Aragón-Salamanca A., Merrifield M. R., 2014, *MNRAS*, **441**, 333
- Kauffmann G., et al., 2003a, *MNRAS*, **341**, 33
- Kauffmann G., et al., 2003b, *MNRAS*, **341**, 54
- Kennicutt Jr. R. C., 1998, *ARA&A*, **36**, 189
- Kovač K., et al., 2010, *ApJ*, **718**, 86
- Larson R. B., Tinsley B. M., Caldwell C. N., 1980, *ApJ*, **237**, 692
- Lilly S. J., Carollo C. M., 2016, *ApJ*, **833**, 1
- Lintott C. J., et al., 2008, *MNRAS*, **389**, 1179
- Marcolini A., Brighenti F., D'Ercole A., 2003, *MNRAS*, **345**, 1329
- Martig M., Bournaud F., Teyssier R., Dekel A., 2009, *ApJ*, **707**, 250
- Mendez A. J., Coil A. L., Lotz J., Salim S., Moustakas J., Simard L., 2011, *ApJ*, **736**, 110
- Moore B., Katz N., Lake G., Dressler A., Oemler A., 1996, *Nature*, **379**, 613
- Mori M., Burkert A., 2000, *ApJ*, **538**, 559
- Nair P. B., Abraham R. G., 2010, *ApJS*, **186**, 427
- Noeske K. G., et al., 2007, *ApJ*, **660**, L43
- Omand C. M. B., Balogh M. L., Poggianti B. M., 2014, *MNRAS*, **440**, 843
- Peng Y.-j., et al., 2010, *ApJ*, **721**, 193
- Peng Y., Maiolino R., Cochrane R., 2015, *Nature*, **521**, 192
- Roberts M. S., Haynes M. P., 1994, *ARA&A*, **32**, 115
- Salim S., 2014, *Serbian Astronomical Journal*, **189**, 1
- Salim S., et al., 2007, *ApJS*, **173**, 267
- Schawinski K., et al., 2014, *MNRAS*, **440**, 889
- Schiminovich D., et al., 2007, *ApJS*, **173**, 315
- Schmidt M., 1968, *ApJ*, **151**, 393
- Skibba R. A., et al., 2009, *MNRAS*, **399**, 966
- Skrutskie M. F., et al., 2006, *AJ*, **131**, 1163
- Smith D. J. B., et al., 2012, *MNRAS*, **427**, 703
- Strateva I., et al., 2001, *AJ*, **122**, 1861
- Teimoorinia H., Bluck A. F. L., Ellison S. L., 2016, *MNRAS*, **457**, 2086
- Wake D. A., van Dokkum P. G., Franx M., 2012, *ApJ*, **751**, L44
- Weinmann S. M., van den Bosch F. C., Yang X., Mo H. J., 2006, *MNRAS*, **366**, 2
- Wetzel A. R., Tinker J. L., Conroy C., 2012, *MNRAS*, **424**, 232
- Woo J., et al., 2013, *MNRAS*, **428**, 3306
- Woo J., Dekel A., Faber S. M., Koo D. C., 2015, *MNRAS*, **448**, 237
- Wright E. L., et al., 2010, *AJ*, **140**, 1868
- Wyder T. K., et al., 2007, *ApJS*, **173**, 293
- York D. G., et al., 2000, *AJ*, **120**, 1579

- da Cunha E., Charlot S., Elbaz D., 2008, [MNRAS](#), **388**, 1595
- de Vaucouleurs G., de Vaucouleurs A., Corwin Jr. H. G., Buta R. J., Paturel G., Fouqué P., 1991, Third Reference Catalogue of Bright Galaxies, Volume I-III.
- van den Bosch F. C., Aquino D., Yang X., Mo H. J., Pasquali A., McIntosh D. H., Weinmann S. M., Kang X., 2008, [MNRAS](#), **387**, 79